Available online at www.sciencedirect.com
SCIENCE DIRECT®
Polymer 44 (2003) 4655–4664
polymer
www.elsevier.com/locate/polymer

# Formation and transformation of hierarchical structure of β-nucleated polypropylene characterized by X-ray diffraction, differential scanning calorimetry and scanning electron microscopy

Jaroslav Ščudla[a], Miroslav Raab[a], Klaus-Jochen Eichhorn[b], Adam Strachota[a,*]

[a]*Institute of Macromolecular Chemistry, Academy of Sciences of the Czech Republic, 162 06 Prague, Czech Republic*
[b]*Institute for Polymer Research, 01069 Dresden, Germany*

Received 24 September 2002; received in revised form 17 March 2003; accepted 25 March 2003

**Abstract**

Commercial grade isotactic polypropylene has been modified with a specific β-nucleant (*N*,*N*′-dicyclohexylnaphthalene-2,6-dicarboxamide) in two concentrations (0.03 and 0.10 wt%). Specimens for structural characterization have been prepared by injection moulding, subsequent melting and re-crystallization or solid-state drawing at 100 °C. Individual levels of hierarchical structure, including molecular orientation, have been characterized by a combination of wide angle X-ray scattering (WAXS), differential scanning calorimetry and scanning electron microscopy. Based on the analysis of the azimuthal reflections (110) and (300), the Hermans orientation functions have been calculated separately for the crystalline phases α and β. Besides the longitudinal orientation along the injection-moulding direction, β-crystallites tilted to the injection-moulding direction have been found. Upon thermal treatment the fraction of the crystalline β-phase has decreased and molecular alignment within the crystalline regions has improved. During solid-state drawing the fraction of the crystalline β-phase was markedly decreasing with increasing draw ratio, while the overall crystallinity has not changed but slightly. The experiments have also revealed a disruption of molecular alignment at the beginning of the drawing process and subsequent distinct improvement of molecular orientation along the draw direction in crystallites α and β. The Hermans orientation functions provided by the WAXS analysis have been compared with recently published data obtained with similar specimens by polarized photoacoustic spectroscopy.


*Keywords:* Isotactic polypropylene; β-Phase of polypropylene; Hermans orientation function

## 1. Introduction

Isotactic polypropylene is a widely used commodity polymer with the fastest production and consumption growth. The reason is its favorable price/performance ratio and many possible modifications. In particular, the application of various nucleating agents (nucleants) is an efficient way to control supermolecular structure. The nucleation of polypropylene has been explored both from technological and scientific points of view. Originally, the nucleants were used as clarifying agents to modify optical properties, later it was shown that they can affect markedly also mechanical properties [1–3]. In particular, specific nucleants can induce spherulite refinement, predominant formation of monoclinic α-phase or less stable hexagonal β-phase. Recent comprehensive study [1] using the same specific β-nucleant as in the present work (*N*,*N*′-dicyclohexylnaphthalene-2,6-dicarboxamide) has revealed that 0.03 wt% is a critical concentration at which the content of the crystalline β-phase reaches a saturation level. At this critical concentration, distinct maxima of toughness, strain at break and long period occurred. In our preceding work [6] we studied the effect of three different specific nucleation agents on supermolecular structure and orientation of isotactic polypropylene. Molecular orientation was studied by polarized photoacoustic Fourier-transform infrared spectroscopy (PPA FTIR) and characterized by the orientation function $f_{PAS}$ derived from characteristic polypropylene bands. Besides, chain orientation within the crystalline regions was studied by wide-angle X-ray diffraction (WAXS) and characterized by orientation factor *O*rel derived from the full width at half maximum (FWHM) of the azimuthal intensity distributions of the characteristic

* Corresponding author. Tel.: +420-296809-264.
*E-mail address:* strachota@imc.cas.cz (A. Strachota).

0032-3861/03/$ - see front matter © 2003 Elsevier Science Ltd. All rights reserved.
doi:10.1016/S0032-3861(03)00287-8

(110) and (300) reflections. Consequently, the interrelation between these two orientation characteristics could not be straightforward.

The objective of the present work is to elucidate the structural formation and transformation of isotactic polypropylene induced by a specific β-nucleant and subsequent history in more detail. The formation and transformation of the crystalline α- and β-phases upon melting, subsequent solidification and annealing is characterized by WAXS, Differential scanning calorimetry (DSC) and Scanning electron microscopy (SEM). The orientation assessed by WAXS is characterized by the Hermans orientation function $f_H$ [4,5]. Thus, the WAXS data could be compared with the values of the 'spectroscopic' orientation function $f_{PAS}$. Moreover, detailed screening of orientation along the neck shoulder of solid-state-drawn specimens allowed the assessment of the dependence of the β-phase content $K_\beta$ and the orientation function $f_H$ on the macroscopic draw ratio λ. The orientation characteristics $f_H$ and $f_{PAS}$ obtained by WAXS and PPA FTIR are compared and discussed for selected typical specimens.

## 2. Experimental

### 2.1. Materials

The starting material used in this study was isotactic polypropylene Mosten 58.412 supplied by Chemopetrol Litvínov, Czech Republic. The manufacturer characterizes the material by the melt flow index of 3 g/10 min (21.2N, 230 °C) and the weight-average molecular weight $M_w$ of about 170,000. The specific β-nucleating agent (β-nucleant) used throughout this work was *N*,*N*′-dicyclohexylnaphthalene-2,6-dicarboxamide, commercial product NJ-Star by Rika International, Manchester, UK. The nucleant has been added to the polypropylene in the form of master batches. The master batches were prepared by premixing polypropylene with 5 wt% of the nucleating agent in a *Brabender Plasticorder*. The master batch of the nucleating agent was then mixed with pellets of isotactic polypropylene in ZE25-CL mixer. The resulting concentrations of the β-nucleant were 0 (PP), 0.03 ($PP\beta_{min}$) and 0.10 wt% ($PP\beta_{max}$).

### 2.2. Specimen preparation, re-crystallization and drawing

Standard dumbbell specimens (DIN 53 455) were prepared by injection moulding in Battenfeld BA 500 CD Plus. The processing conditions were described elsewhere [6].

Some of the injection-moulded specimens were additionally exposed to re-crystallization. The specimens were tightly wrapped in an aluminium foil to preserve their shape and left for 60 min at 210 °C in an oven to melt. The specimens were then immediately moved into another oven and kept for additional 60 min at 123 °C. After annealing the specimens were slowly cooled to room temperature. Similar temperature history was also performed in a DSC cell with samples cut out of the core portion of the original injection-moulded specimens. The DSC samples were quickly heated (80 K $min^{-1}$) to 210 °C, left for 60 min in the melted state and then quickly cooled (80 K $min^{-1}$) to the crystallization temperature of 123 °C. After 60 min of annealing at that temperature, the samples were slowly cooled (10 K $min^{-1}$) to room temperature. (It was reported [3] that radial growth of β-spherulites reaches a maximum just around 123 °C).

In addition, some original injection-moulded specimens were subsequently drawn in the temperature chamber of a Zwick 1456 Tensile Tester at 100 °C and drawing speed of 20 mm $min^{-1}$. Equidistant ink marks (5 mm distance) were introduced along the gauge length to assess the local drawing ratio λ of the drawn specimens. Before the drawing started, the specimens were clamped in the grips of the tensile tester and left for 30 min in the closed temperature chamber at 100 °C. After the test the specimens were kept another 30 min in the grips to relax in the chamber at the same temperature and only then slowly cooled to room temperature in the opened chamber. The chamber dimensions allowed the specimens to be drawn to the maximal extension of $\Delta l = 200$ mm ($\epsilon_{max} = 2.0$).

### 2.3. Wide-angle X-ray scattering

A diffractometer P4 (Bruker, Karlsruhe) using Cu Kα radiation (monochromatized with primary graphite crystal) was used for the WAXS analysis of all studied materials. The diffractometer measured, within radial scattering range $2\theta$ from 1.5 to 40.5°, in the transmission mode with area detection system HiStar/GADDS. The diameter of the detector pin hole was 0.5 mm (with distance 12 cm between the sample and detector) and the measurement time was 180 s. The resulting standard two-dimensional scattering patterns were evaluated by a procedure described elsewhere [6]. An example of a typical diffraction pattern (one quadrant) for the specimen nucleated with 0.03 wt% of β-nucleant is shown in Fig. 1.

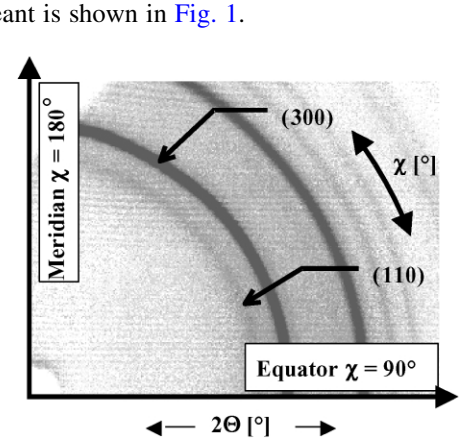


Fig. 1. Diffraction pattern of the specimen nucleated with 0.03 wt% of β-nucleant ($PP\beta_{min}$). Indicated are the reflections (110) and (300) corresponding to the crystalline phases α and β, respectively.

The overall crystallinity $X_c$ has been calculated by integration of the diffraction patterns in one quadrant as all the studied materials showed quadrant symmetry. At the same time an experimental error of this estimation has been evaluated from the difference between the real and approximated intensity profiles. The relative amount of the β-phase $K_\beta$ in the crystalline portion of the material has been evaluated by the method of Turner-Jones et al. [7]

$$K_\beta = \frac{I_\beta}{I_{\alpha 1} + I_{\alpha 2} + I_{\alpha 3} + I_\beta} \tag{1}$$

where $I_\beta$ is the integral intensity of (300) reflection of the β-phase, and $I_{\alpha 1}$, $I_{\alpha 2}$, and $I_{\alpha 3}$ are the integral intensities of the (110), (040) and (130) reflections of the α-phase, respectively. The orientation of both α- and β-crystalline phases has been evaluated for the original and re-crystallized injection-moulded specimens and along the drawn specimens at sites of different local draw ratios $\lambda$. For such determination individual sections of different draw ratios $\lambda$ have been cut from the neck shoulder of the drawn specimens and subsequently cleaved in liquid nitrogen along the draw direction. The thickness of the resulting samples for the WAXS analysis was 1–2 mm. In our previous work [6] a relative parameter $O_{rel}$ derived from the WAXS data was used for characterization of molecular orientation as a function of FWHM

$$O_{rel} = \frac{180^\circ - \mathrm{FWHM}}{180^\circ} \in (0;1) \tag{2}$$

However, this parameter is not sensitive enough to real orientation and the relation between $O_{rel}$ and the Hermans orientation function $f_H$ is non-linear as shown in Fig. 2.

Therefore a more complex procedure was adopted in the present work allowing a direct estimation of the Hermans orientation function $f_H$. According to definition [4]

$$f_H = \frac{3\,\overline{\cos^2\chi} - 1}{2} \tag{3}$$

where $\chi$ is the angle between the polymer chain segment and preferred orientation (injection-moulding direction or drawing direction). The average value of $\overline{\cos^2\chi}$ is given by integration using the equation [5]

$$\overline{\cos^2\chi} = \frac{\int_0^{\pi/2} I_{hkl}(\chi)\cos^2\chi\sin\chi\,\mathrm{d}\chi}{\int_0^{\pi/2} I_{hkl}(\chi)\sin\chi\,\mathrm{d}\chi} \tag{4}$$

where $\chi$ is the azimuthal angle of the diffraction pattern. After performing the Lorentzian fitting procedure for an experimental diffraction peak, we get

$$I_{hkl} = \frac{2A}{\pi}\frac{\mathrm{FWHM}}{4(\chi-\chi_o)^2 + \mathrm{FWHM}^2} \tag{5}$$

where $A$ is total area under the Lorentzian curve, $\chi_o$ is the centre of the peak (corresponding to the preferential direction), FWHM is full width of the peak at half maximum, which is identical for the experimental and fitted curves. Inserting experimental azimuthal intensity distributions $I_{110}$ and $I_{300}$ of the (110), and (300) reflections, respectively, for the general distribution $I_{hkl}$, the orientation functions for the crystalline phases α and β have been calculated.

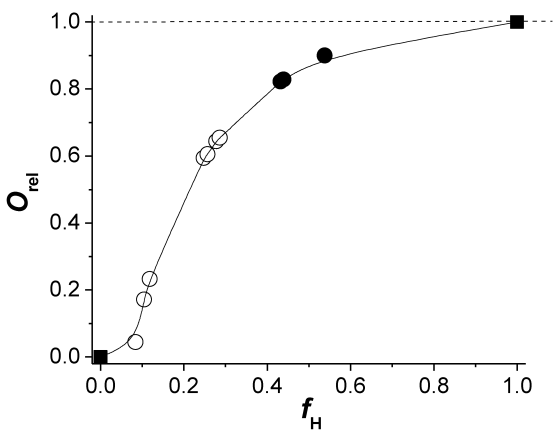


Fig. 2. The relation between two characteristics of molecular orientation, $O_{rel}$ and $f_H$. Data points represent the values calculated for real oriented specimens, injection-moulded (○) or drawn (●). Both characteristics approach limit values 0 or 1 for randomly oriented systems or perfectly oriented systems, respectively (■).

### 2.4. Differential scanning calorimetry

DSC thermograms were measured by a Perkin–Elmer DSC 7 (equipped with a software *Pyris*, version 3.51) over the temperature range of 10–210 °C. Heating rate was 10 K min$^{-1}$ for the study of structural transformation and 40 K min$^{-1}$ for the assessment of the β-phase content $K_\beta$. Representative samples containing both core and skin regions were cut out from the injection-moulded or subsequently re-crystallized specimens. The procedure for the assessment of crystallinity $X_c$ and the content of the β-phase $K_\beta$ has been described in our preceding paper [6].

### 2.5. Scanning electron microscopy

SEM VEGA (Tescan Brno, Czech Republic) was used for morphology assessment. Cross-sections of the specimens perpendicular to the long axes were scratched with glass edge in liquid nitrogen to obtain flat surfaces without affecting the morphology. For contrasting the crystalline morphology, permanganic etching was used as described by Aboufaraj et al. [8]. After etching the surface was washed for 15 min by distilled water and subsequently cleaned for 15 min with acetone in ultrasound bath. Secondary electron mode was used for imaging with 30 kV acceleration voltage

of the primary scanning beam. Specimen tilt was 30° in all cases.

## 3. Results and discussion

### 3.1. The effect of thermal treatment

The basic morphological characteristics as assessed by WAXS, DSC and SEM were studied with original injection-moulded specimens and the same specimens after re-crystallization and subsequent annealing. The quantitative results are summarized in Table 1. For injection-moulded specimens it can be seen that the specific nucleation does not significantly influence the overall crystallinity $X_c$, but enhances dramatically the relative content $K_\beta$ of the β-phase. The higher nucleant content (0.10 wt%) has brought about a small but significant increase in $K_\beta$ as compared with the sample with a lower nucleant concentration (0.03 wt%). The X-ray and DSC data are in reasonable agreement within the experimental scatter. It should be noted that WAXS data were obtained for the overall thickness of the specimens. Thus, the data are an average of skin and core morphology. (The results of a previous study [6] on similar systems showed significantly higher β-phase contents in the core regions of injection-moulded specimens.)

After melting, solidification and annealing in an oven, the overall crystallinity $X_c$ of all specimens increased but the relative fraction of the β-phase, $K_\beta$ markedly decreased. Surprisingly, this decrease was more pronounced for the specimen with higher nucleant content (PP$\beta_{max}$). These results indicate that the formation of the crystalline β-phase is controlled not only by the presence of the specific nucleant itself but also by the thermal history during injection moulding. The important effect of the cooling rate during solidification from the melt is demonstrated by the DSC thermograms in Fig. 3 for the sample nucleated with higher nucleant content (PP$\beta_{max}$). The two main endotherms of the original injection-moulded specimens

Table 1
Comparison of WAXS and DSC data for injection-moulded specimens and specimens after re-crystallization. Thermal treatment in an oven and in a DSC cell are indicated by symbol (o) and (c), respectively. The experimental error values of the WAXS data reflect deviations of the real diffractograms from the fitted curves

| Material | $X_c$ (%) | | $K_\beta$ (%) | |
|---|---|---|---|---|
| | WAXS | DSC | WAXS | DSC |
| PP | 58 ± 5 | 53 | 0 | 0 |
| PP$\beta_{min}$ | 57 ± 6 | 50 | 68 ± 6 | 62 |
| PP$\beta_{max}$ | 60 ± 7 | 51 | 83 ± 7 | 72 |
| PP$\beta_{min}$ (o) | 65 ± 5 | – | 45 ± 5 | – |
| PP$\beta_{max}$ (o) | 66 ± 4 | – | 34 ± 4 | – |
| PP$\beta_{max}$ (c) | 63 ± 6 | 56 | 92 ± 6 | 89 |

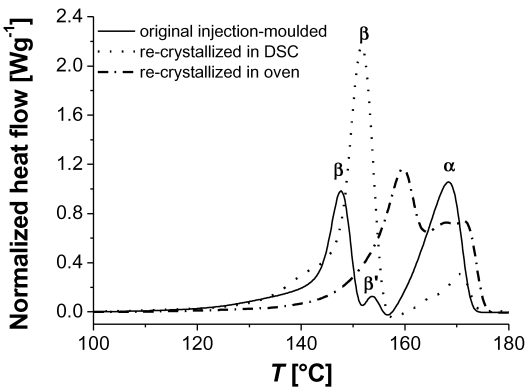


Fig. 3. DSC thermograms of polypropylene samples of different thermal history nucleated with 0.1% of β-nucleating agent (PP$\beta_{max}$). Heating rate 10 K min$^{-1}$.

obviously correspond to the melting of the β-phase ($T_m$ = 148 °C) and of the α-phase ($T_m$ = 168 °C). The small intermediate peak $\beta'$ located at 153.5 °C reflects the re-crystallization of the original β-phase into a more ordered structure as already discussed [6,9]. The specimen exposed to re-crystallization and subsequent annealing in oven shows again two main endotherms. However, the peak located at 160 °C could not be ascribed to pure crystalline β-phase but rather to melting of a more complex structure containing both α and β crystallites. It should be noted, that the intensity of this peak suggests a higher β-phase content, $K_\beta$, than determined by the WAXS analysis (see Table 1). The double peak located at about 170 °C reflects the presence of a complex α-phase and its possible re-crystallization. Finally, the sample re-crystallized at a relatively high cooling rate (80 K min$^{-1}$) directly in the DSC cell shows predominant endotherm of the β-phase located at 152 °C and only a small α-phase endotherm at 171 °C. In this case the fast cooling favored the formation of well-ordered β-phase as indicated also by the WAXS analysis (see Table 1).

Scanning electron microscopy has shown that the nucleation and thermal treatment of the examined samples influenced not only the crystalline structure but also the spherulitic morphology. This is documented by Figs. 4(a)–(d). Several morphological observations can be derived from these figures: first, the original injection-moulded material prepared without any nucleant (PP) contains well-developed α-spherulites of about 15 μm in diameter (Fig. 4(a)). Second, the specimen PP$\beta_{min}$ prepared with the lower nucleant concentration (0.03%) shows bundle-like morphology without developed spherulites. Third, the specimen PP$\beta_{max}$ prepared with a higher nucleant concentration (0.10%) shows a structure with well-developed spherulites distinctly different from the α-spherulites in neat polypropylene. The results of WAXS suggest that these objects with characteristic coarse morphology are β-spherulites. Fourth, after thermal treatment, some of the coarse spherulites are replaced by characteristic α-spherulites (Fig. 4(d)). This morphological observation is in

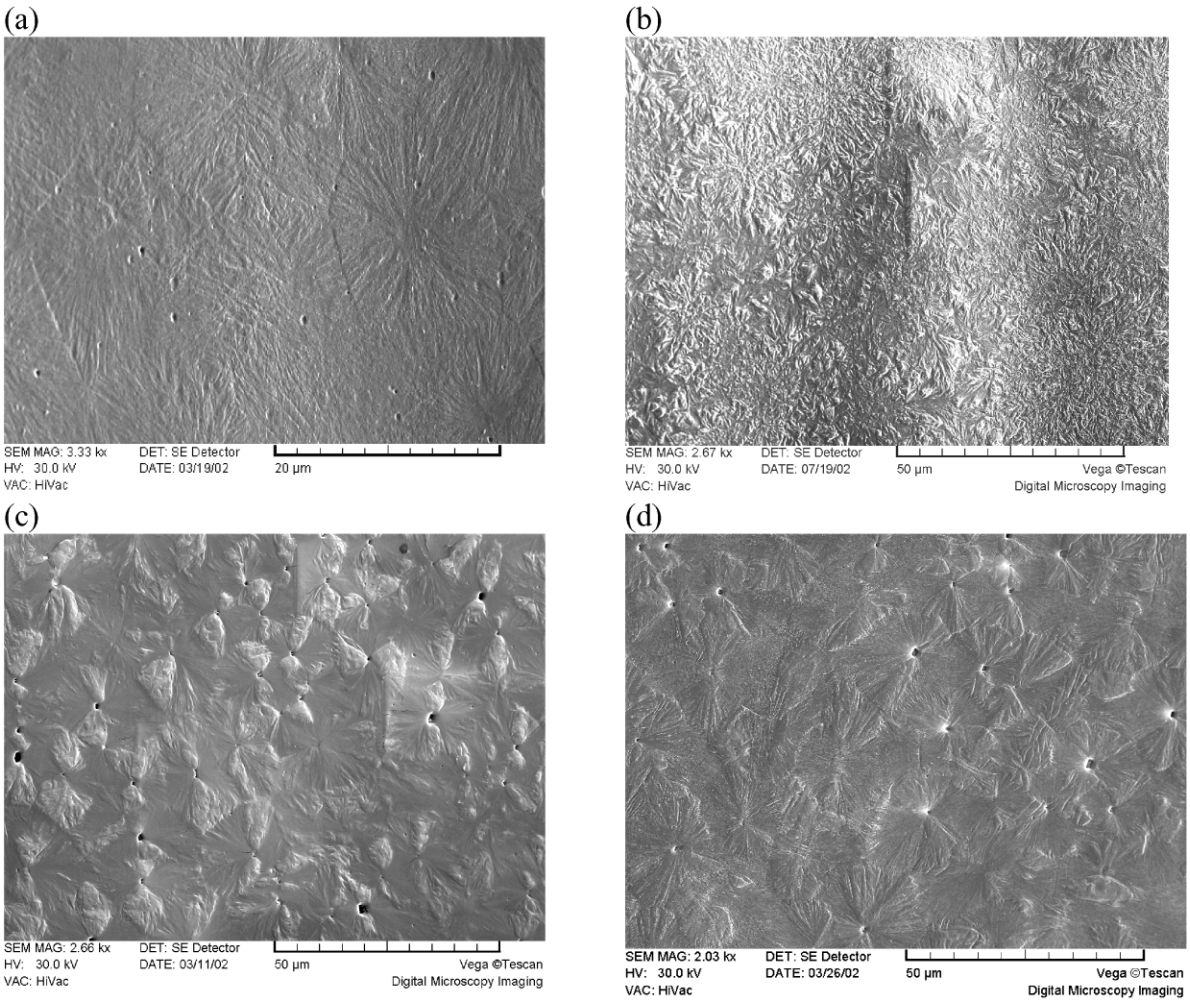


Fig. 4. Scanning electron micrographs of the investigated materials used in this work: (a) PP, (b) PPβ$_{min}$, (c) PPβ$_{max}$, (d) re-crystallized PPβ$_{max}$.

agreement with the WAXS data showing a distinct decrease in the β-phase content. Different supermolecular morphology revealed by scanning electron microscopy of the specimens differing in nucleant content might explain their different mechanical behaviour [1]. We might suggest that the presence of β-crystallites on one hand, but suppressed spherulite formation on the other, are favorable for higher plasticity and toughness with the specimens modified with a 'critical' nucleant content (0.03 wt%).

Generally, the nucleation has brought about a certain spherulite refinement. The sizes of the spherulites in nucleated specimens were ca. 10 μm as compared to some 15 μm with neat polypropylene (PP). In the case of specimens with the higher nucleant content (PPβ$_{max}$), the permanganic etching has revealed imprints of nucleant particles in the central part of some typical β-spherulites. Individual angular particles of the β-nucleant have typically dimensions of about 0.5–1.0 μm. It is interesting, however, that no nucleant imprints could be seen in the structure of the specimen with the lower nucleant content (PPβ$_{min}$).

The original injection-moulded specimens have already shown certain molecular orientation. Analysis of azimuthal intensity distributions made it possible to separately evaluate the orientation for the crystalline phases α and β. In Fig. 5(a), left, it is shown that molecular orientation within the α-crystallites is relatively weak with partial orientation along and across the axes of the injection-moulded specimens. The corresponding diffraction maxima are indicated as $\alpha_{\parallel}$ and $\alpha_{\perp}$. As shown in Fig. 5(b), left, the longitudinal orientation within the α-crystallites is preserved, even after thermal treatment, but the cross orientation remains only in the specimen with a higher nucleant content (PPβ$_{max}$). The overall increase in the α-phase content is reflected in the shift of the profile towards higher intensity values.

The molecular orientation in the β-phase is more pronounced and more complex (Fig. 5(a), right). The azimuthal profile indicates distinct longitudinal orientation for the specimen with lower nucleant content (PPβ$_{min}$). The equatorial azimuthal maximum ($\beta_E$) of the specimen with a higher nucleant content (PPβ$_{max}$) indicates again the longitudinal orientation within the β-phase, but two additional maxima appear ($\beta_{A1}$, $\beta_{A2}$, forming an M-shaped profile) located at angles $\pm 30°$

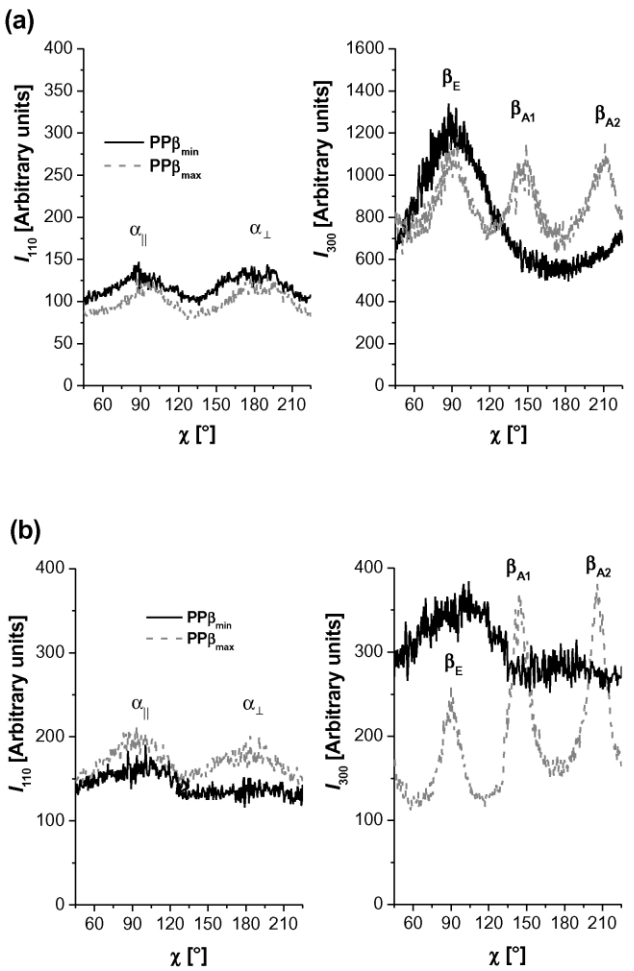


Fig. 5. Azimuthal intensity distributions for injection-moulded specimen (a) and specimens after thermal treatment (b). The reflections (110) left and (300) right characterize the molecular orientation within the crystalline phases α and β, respectively. Equator $\chi = 90°$, meridian $\chi = 180°$.

from meridian ($\chi = 180°$). These maxima seem to indicate the presence of a system of β-crystallites with molecular chains symmetrically inclined to the specimen axes. Even if the overall content of β-phase decreases after thermal treatment, this complex orientation order is not only preserved but even more developed (Fig. 5(b), right). These results illustrate the memory effect in polymer melts.

For each azimuthal diffraction maximum mentioned above, the values $f_H$ of the Hermans [4,5] orientation function have been calculated. The results are summarized in Table 2. The presence of β-crystallites with molecular orientation somewhat inclined to specimen axis, especially with re-crystallized specimens, is again well demonstrated. The corresponding diffraction maxima in azimuthal representation are shifted by $\pm 30°$ from the meridian. In this case the values of the orientation function $f_H$ were related to the preferential direction $\chi_o$ (Eq. (5)). These diffraction maxima correspond to the same axially symmetrical system of

Table 2
The values of Hermans orientation function $f_H$ calculated for individual azimuthal reflections of injection-moulded and subsequently re-crystallized specimens containing 0.03 wt% ($PP\beta_{min}$) and 0.10 wt% ($PP\beta_{max}$) of specific β-nucleant

| Reflection | Specimen | | | |
|---|---|---|---|---|
| Maximum | Injection-moulded | | Re-crystallized | |
| | $PP\beta_{min}$ | $PP\beta_{max}$ | $PP\beta_{min}$ | $PP\beta_{max}$ |
| $\alpha_{\parallel}$ | 0.294 | 0.201 | 0.121 | 0.201 |
| $\alpha_{\perp}$ | 0.195[a] | 0.182[a] | – | 0.142[a] |
| $\beta_E$ | 0.209 | 0.335 | 0.109 | 0.445 |
| $\beta_{A1}$ | – | 0.364[a] | – | 0.514[a] |
| $\beta_{A2}$ | – | 0.361[a] | – | 0.510[a] |

[a] The orientation functions $f_H$ corresponding to the reflection maximum $\alpha_{\perp}$ were related to the direction perpendicular to the specimen axes. For the reflection maxima $\beta_{A1}$, $\beta_{A2}$, the values of the orientation function $f_H$ were related to preferential directions tilted to the specimen axis.

β-crystallites. Indeed, the values of the orientation functions $f_H$ corresponding to these reflection maxima labelled as $\beta_{A1}$, $\beta_{A2}$ are virtually identical within experimental scatter.

### 3.2. The effect of solid-state drawing

Since the pioneering work of Turner-Jones et al. [7], the effect of mechanical loading and deformation on the transformation of the crystalline β-phase into a more stable α-phase has been studied experimentally and discussed theoretically by several authors [10,11]. In particular, the β–α transformation under dynamic conditions has been suggested as one of possible explanations of the enhanced toughness of β-modified polypropylene. More recently, this transition during cold drawing has been followed by DSC [12]. The approach of the present work made it possible to monitor the structural transformation during solid-state drawing by WAXS analysis for specimens modified with the specific β-nucleant of two concentrations (0.03, 0.10 wt%). The temperature of 100 °C has been selected for the drawing experiment in order to suppress stress whitening. This temperature is close to the optimum drawing temperature for polypropylene (110 °C) [13]. While the process of molecular orientation of neat polypropylene during solid-state drawing is highly heterogeneous and concentrated in a narrow neck shoulder, the neck region of β-modified polypropylene is extended and

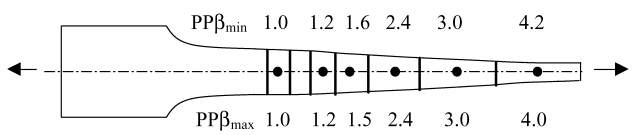


Fig. 6. Schematic representation of individual samples for WAXS analysis taken from the neck region of drawn specimens. The values of the local draw ratio λ for the specimen with lower and higher nucleant concentration are indicated along the neck shoulder.

flat. As shown schematically in Fig. 6, six locations with different local draw ratios λ were selected for the structural characterization by WAXS analysis. The values of the local draw ratios λ differed slightly depending on the nucleant content. The analysis of WAXS diffraction patterns in one quadrant by a procedure described elsewhere [6] yielded the β-phase content $K_\beta$ and overall crystallinity $X_c$.

The values of $K_\beta$ and $X_c$ versus the local draw ratio λ are plotted in Fig. 7. It can be seen that the β-phase content $K_\beta$ monotonically decreases with increasing λ while the overall crystallinity $X_c$ remains virtually constant within experimental scatter. These results are in good qualitative agreement with data of Li and Cheung [12] obtained by DSC for samples with initial β-phase content $K_\beta = 61\%$.

The effect of the local draw ratio λ on the azimuthal intensity distributions is shown in Fig. 8 separately for the reflection (110) corresponding to the α-phase and for the reflection (300) corresponding to the β-phase. The increasing intensity of the $\alpha_{\parallel}$-maximum with increasing draw ratio reflects improving molecular orientation for both nucleant concentrations (Fig. 7(a),(b)). On the other hand, the maxima $\alpha_{\perp}$ indicating molecular orientation in the cross direction became insignificant upon drawing. Obviously, solid-state drawing improves the molecular orientation solely along the draw direction.

The development of the diffraction profiles corresponding to the crystalline β-phase is more complex and differs for lower and higher nucleant contents (Fig. 8(c),(d)). Several observations should be noted: first, the general decrease of the intensity of the (300) reflection with increasing draw ratio λ correspond the decrease in the β-phase content $K_\beta$. Second, the orientation within the β-crystallites is markedly disrupted at a low draw ratio ($\lambda = 1.6$), especially for the lower nucleant content ($PP\beta_{min}$). This observation seems to support the notion of the destruction of pre-existing crystalline regions, that is, melting, during cold drawing, as suggested by Flory and Yoon [14]. Indeed, melting spots together with shear bands were found by Li et al. [15] in a yielded polypropylene sample. Third, a distinct equatorial maximum occurs again

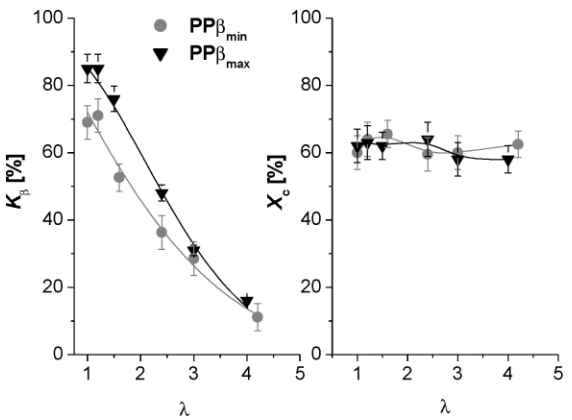


Fig. 7. The effect of local draw ratio λ on the fraction of the β-phase $K_\beta$ (left) and the overall crystallinity $X_c$ (right).

for the highest draw ratio ($\lambda \sim 4.0$). However, in this case a contribution of the equatorial maximum of the (110) reflection (α-phase) might influence the intensity of this (300) reflection corresponding to the β-phase. Fourth, the additional diffraction maxima forming an M-shaped profile ($\beta_{A1}$, $\beta_{A2}$) for the higher nucleant content ($PP\beta_{max}$), as discussed above, gradually disappeared, with increasing draw ratio λ. For the highest obtained draw ratio ($\lambda = 4.0$), only molecular orientation along the draw direction is preserved within the β-crystallites. We might suppose that the β-crystallites originally tilted to the specimen axis were preferentially transformed to the α-phase.

The Hermans orientation functions $f_H$ calculated from the individual diffraction maxima discussed above are plotted in dependence on the draw ratio λ in Fig. 9. The minimum of the molecular orientation at lower draw ratio λ for the sample with lower nucleant content ($PP\beta_{min}$) and the disappearance of the tilted β-crystallites at the highest draw ratio for the sample with higher nucleant content ($PP\beta_{max}$) is demonstrated. Again, the above results reflect the disruption of the supermolecular structure upon drawing, followed by recrystallization, as theoretically predicted [14,16].

Development of a computing procedure for the assessment of Hermans orientation function $f_H$ from WAXS diffraction patterns has been an original contribution of this work. The procedure is illustrated in Fig. 10(a) for a complex case of the sample $PP\beta_{max}$ and the local draw ratio $\lambda = 2.4$. Here, the equatorial maximum at 90° and two maxima of the M-shaped profile at about 150 and 210° could be seen. Before calculation, the background intensity $I_0$ (amorphous halo) had to be subtracted. As shown in Fig. 10(b), the value $I_0$ has been obtained from the radial intensity diffraction profile. The azimuthal diffraction maxima were then fitted by the Lorentzian functions $I_{hkl}$ (Eq. (5)). Subsequently, the Hermans orientation functions $f_H$ have been calculated using Eqs. (3) and (4).

### 3.3. Comparison of X-ray and spectroscopic data on orientation

Characterization of orientation by the Hermans orientation function $f_H$ made it possible to compare the data obtained by the WAXS analysis with previously published data [6] of PPA FTIR. The values of the orientation functions $f_H$ calculated for individual azimuthal diffraction peaks of injection-moulded and subsequently drawn specimens are summarized in Table 3 together with the values of orientation functions $f_{PAS}$ detected spectroscopically for skin and core regions of equivalent specimens. Both methods measured the orientation in different ways. While the WAXS analysis detects the average orientation through the thickness of the specimen, the infrared spectroscopy measures the orientation of surface layer approximately 20 μm thick. What is even more important, the WAXS analysis measures orientation separately in the α and β

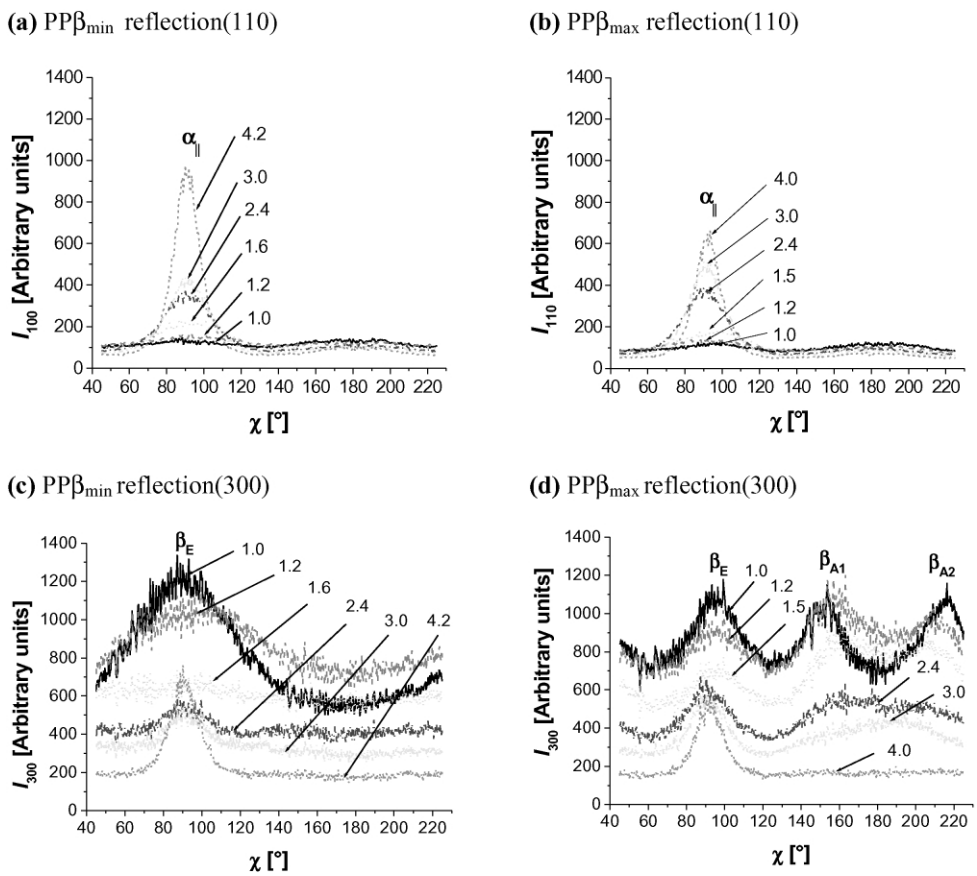


Fig. 8. Azimuthal intensity distributions of the reflections (110) and (300) of the β-modified polypropylene nucleated with β-nucleating agent at two different concentrations. (The labelling of individual maxima is the same as in Fig. 5, local values of draw ratio $\lambda$ are indicated at individual curves.) Equator $\chi = 90°$, meridian $\chi = 180°$.

phases. On the other hand, in the case of spectroscopic investigation, the surface (skin), and the inner part of the investigated specimens (core) were measured separately on split specimens [17,18]. As the WAXS data characterize the orientation within the crystalline phase, the spectroscopic orientation functions $f_{PAS}$ selected for the comparison were calculated from the 998 $cm^{-1}$ band. It has been recognized that this band reflects the orientation in the crystalline phase [19]. The results summarized in Table 3 show that the data correlate relatively well for the injection-moulded specimens, where β-phase prevails. The very low orientation detected by the PPA FTIR in the core region ($f_{PAS} = 0.04$) for the specimen PPβ$_{max}$ can be explained by the counter effect of the two differently oriented β-phases (see Table 3).

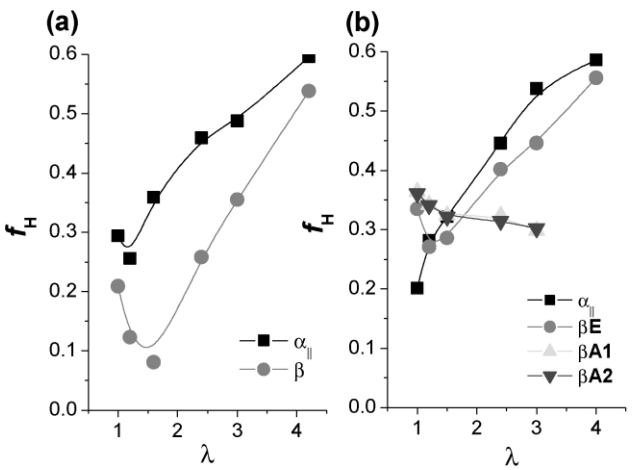


Fig. 9. Orientation functions of α- and β-phases in β-nucleated specimens *versus* draw ratio λ: (a) PPβ$_{min}$ (b) PPβ$_{max}$. The symbols correspond to those in Fig. 8. The values of the orientation function $f_H$ were related to the specimen axis, except for the reflection maxima $\beta_{A1}$, $\beta_{A2}$, where the orientation functions $f_H$ were related to the preferential direction $\chi_o$ tilted to the specimen axis (Eq. 5).

For the specimen portions drawn to the highest draw ratio ($\lambda = 4.2$ for PPβ$_{min}$ and $\lambda = 4.0$ for PPβ$_{max}$), the values of the spectroscopic orientation function are distinctly higher than that found by the WAXS determination, especially for the skin. This might indicate that spectroscopy reflects orientation of some intermediate phase, which X-ray analysis cannot assess as a distinct α- or β-phase. Obviously, infrared spectroscopy is sensitive to a short-range order of stretched polymer chains or chain segment outside of the α- or β-crystalline phases. In other words, an orientation in three-dimensional crystalline lattice is necessary to be detected by X-ray diffraction, while infrared spectroscopy can assess also a one-dimensional orientation in less ordered (fibre-like) structure.

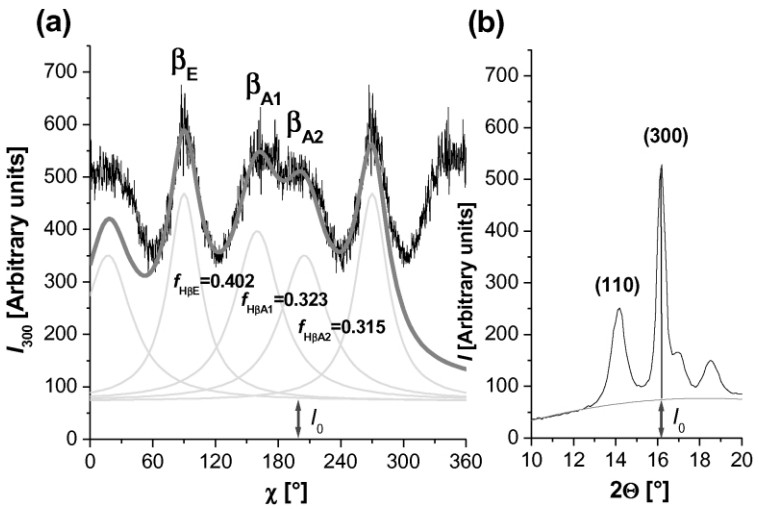


Fig. 10. An example of assessment of orientation functions $f_H$ for sample PP$\beta_{max}$ and draw ratio $\lambda = 2.4$. (a) Approximation of the experimental azimuthal intensity distribution $I_{300}$ for the β-reflection (300) by a set of theoretical Lorentzian distributions. (b) Corresponding radial intensity distribution $I$ showing characteristic reflections of the α-phase (110) and β-phase (300). The arrows indicate the subtraction of background intensity $I_0$ (amorphous halo).

## 4. Conclusions

Several conclusions on formation and transformation of supermolecular structure could be drawn from the experimental results of this work:

1. The study revealed the effect of thermal history on the efficiency of a specific β-nucleant applied in two concentrations (0.03 and 0.10 wt%). These two concentrations induced the formation of 70–80% of the crystalline β-phase in injection-moulded specimens but only about one half of this modification remained in specimens after re-melting and subsequent annealing. On the other hand, fast cooling in the DSC cell induced the formation of more than 90% as indicated also by WAXS analysis.
2. Computation procedure was developed yielding directly the values of Hermans orientation functions from the analysis of azimuthal WAXS reflections. The procedure is based on deconvolution of experimental diffraction profiles by theoretical Lorentzian functions. Thus, the WAXS data could be directly compared with the orientation characteristics obtained by polarized photoacoustic FTIR spectroscopy.
3. Molecular orientation in injection-moulded specimens was assessed separately for crystalline phases α and β. Prevailing uniaxial orientation along the specimen axis was established within the α-crystallites and a more complex supermolecular structure was found for the β-phase. For specimens with higher contents of the β-nucleant, two diffraction maxima located at angles ± 30° from meridian, in addition to the equatorial maximum, were found. These additional maxima became even more pronounced after re-crystallization. Different supermolecular morphology as revealed by scanning electron microscopy of the specimens differing in nucleant content might explain their different mechanical behavior. It is suggested that the presence of β-crystallites on one hand, but suppressed spherulite formation on the other, is advantageous for higher plasticity and toughness with the specimens modified with a 'critical' nucleant content (0.03 wt%).
4. WAXS analysis performed along neck shoulder of drawn specimens revealed a disruption of oriented structures at low draw ratio ($\lambda = 1.6$) followed by a marked improvement of molecular orientation along the draw direction both in the α- and β-phases. At the same time, the content of the β-phase monotonically decreases with increasing draw ratio.

Table 3
The orientation functions assessed by WAXS ($f_H$) and PPA FTIR ($f_{PAS}$) of polypropylene nucleated by two concentrations of β-nucleant

| Specimen processing | Sample | λ | WAXS | | | | PPA | FTIR |
|---|---|---|---|---|---|---|---|---|
| | | | $\alpha\|\|$ | $\beta_E$ | $\beta_{A1}$ | $\beta_{A2}$ | Skin | Core |
| Injection moulding | PP$\beta_{min}$ | 1.0 | 0.294 | 0.209 | – | – | 0.22 | 0.10 |
| | PP$\beta_{max}$ | 1.0 | 0.201 | 0.335 | 0.364[a] | 0.361[a] | 0.37 | 0.04 |
| Subsequent drawing | PP$\beta_{min}$ | 4.2 | 0.596 | 0.538 | – | – | 0.89 | 0.73 |
| | PP$\beta_{max}$ | 4.0 | 0.586 | 0.556 | – | – | 0.93 | 0.74 |

[a] The orientation functions $f_H$ corresponding to the reflection maximum $\alpha_\perp$ were related to the direction perpendicular to the specimen axes. For the reflection maxima $\beta_{A1}$ and $\beta_{A2}$, the values of the orientation function $f_H$ were related to the preferential direction $\chi_o$ tilted to the specimen axis (Eq. (5)).

5. A complex hierarchical structure of injection-molded and subsequently solid-state-drawn specimens was revealed by comparison of orientation functions obtained by WAXS and PPA FTIR spectroscopy. Very low orientation in the core of injection-molded specimens modified with a higher nucleant content as indicated by PPA FTIR might be explained by mutual compensation of differently oriented β-crystallites. On the other hand, the spectroscopy indicated significantly higher orientation for the drawn specimens than WAXS analysis.

## Acknowledgements

This work was supported by the Grant Agency of the Czech Republic (project No. 106/ 02/1249) and by the Saxonian Government (project SMWK-Az. 4-7531.50-04-821-00/7) during the stay of one of the authors (J.Š.) at the Institute for Polymer Research in Dresden. The authors also thank Dr Ladislav Pospíšil, Polymer Institute Brno for donation of nucleant sample. Thanks are also due to Drs P. Schmidt and J. Baldrian, IMC Prague and Dr D. Jehnichen and L. Häußler, IPF Dresden for their useful advice and discussion.

## References

[1] Kotek J, Raab M, Baldrian J, Grellmann W. J Appl Polym Sci 2002; 85(6):1174–84.
[2] Tjong SC, Shen JS, Li RKY. Polym Engng Sci 1996;36(1):100–5.
[3] Tordjeman P, Robert C, Marin G, Gerard P. Eur Phys J E 2001;4: 459–65.
[4] Hermans PH. In: Hermans JJ, editor. Contribution to the Physics of Cellulose Fibers. Amsterdam: Elsevier; 1946. Appendix III.
[5] Alexander LE. X-ray Diffraction Methods in Polymer Science. New York: Wiley; 1969. p. 243.
[6] Ščudla J, Eichhorn KJ, Raab M, Schmidt P, Jehnichen D, Häußler L. Macromol Symp 2002;184:371–87.
[7] Turner JVA, Aizlewood JM, Beckett DR. Makromol Chem 1964;75: 134–58.
[8] Aboufaraj M, Ulrich B, Dahoun A, G'Sell C. Polymer 1993;34(23): 4817–25.
[9] Kotek J, Kratochvíl J, Baldrian J, Raab M. Macromol Symp, in press.
[10] Karger-Kocsis J, Varga J, Ehrenstein GW. J Appl Polym Sci 1997; 64(11):2057–66.
[11] Karger-Kocsis J, Varga J. J Appl Polym Sci 1996;62(2):291–300.
[12] Li JX, Cheung WL. Polymer 1998;39(26):6935–40.
[13] Wills AJ, Cappacio G, Ward IM. J Polym Sci Polym Phys Ed 1980;18: 493–509.
[14] Flory PJ, Yoon DY. Nature 1978;272:226–9.
[15] Li JX, Cheung WL, Chan CM. Polymer 1999;40:2089–102.
[16] Juska T, Harrison IR. Polym Engng Sci 1982;22:766–76.
[17] Schmidt P, Dybal J, Ščudla J, Raab M, Kratochvíl M, Eichhorn KJ, López Quintana S, Pastor JM. Macromol Symp 2002;184:107–22.
[18] Schmidt P, Baldrian J, Ščudla J, Dybal J, Raab M, Eichhorn KJ. Polymer 2001;42(12):5321–6.
[19] Kobayashi Y, Okajima S, Narita A. J Appl Polym Sci 1967;11: 2515–23.